International Journal of Lightweight Materials and Manufacture 3 (2020) 387–402

Contents lists available at ScienceDirect

International Journal of Lightweight Materials and Manufacture

journal homepage: https://www.sciencedirect.com/journal/international-journal-of-lightweight-materials-and-manufacture

Underwater blast loading of partially submerged sandwich composite materials in relation to air blast loading response

Emily Rolfe [a], Robert Quinn [a], George Irven [a, b], David Brick [c], John P. Dear [a], Hari Arora [d, *]

[a] Department of Mechanical Engineering, Imperial College London, London, SW7 2AZ, UK
[b] FAC Technology, 53 Lydden Grove, Wandsworth, London, SW18 4LW, UK
[c] Radnor Range Ltd, 11 Broadaxe Business Park, Presteigne, LD8 2UH, UK
[d] Zienkiewicz Centre for Computational Engineering, College of Engineering, Swansea University, Swansea, SA1 8EN, UK

ARTICLE INFO

Article history:
Received 28 February 2020
Received in revised form
18 May 2020
Accepted 5 June 2020
Available online 15 June 2020

Keywords:
Underwater blast
Air blast
Composite sandwich panel
Hybrid composite
Digital image correlation

ABSTRACT

The research presented in this paper focusses on the underwater blast resilience of a hybrid composite sandwich panel, consisting of both glass-fibre and carbon-fibre. The hybrid fibres were selected to optimise strength and stiffness during blast loading by promoting fibre interactions. In the blast experiment, the aim was to capture full-field panel deflection during large-scale underwater blast using high-speed 3D Digital Image Correlation (DIC). The composite sandwich panel was partially submerged and subjected to a 1 kg PE7 charge at 1 m stand-off. The charge was aligned with the centre of the panel at a depth of 275 mm and mimicked the effect of a near-field subsurface mine. The DIC deflection data shows that the horizontal cross-section of the panel deforms in a parabolic shape until excessive deflection causes core shear cracking. The panel then forms the commonly observed “bathtub” deformation shape. DIC data highlighted the expected differences in initial conditions compared to air-blast experiments, including the pre-strains caused by the mass of water (hydrostatic pressure). Furthermore, water depth was shown to significantly influence panel deflection, strain and hence damage sustained under these conditions. Panel deformations and damage after blast was progressively more severe in regions deeper underwater, as pressures were higher and decayed slower compared to regions near the free surface.

An identical hybrid composite sandwich panel was subjected to air blast; one panel underwent two 8 kg PE7 charges in succession at 8 m stand-off. DIC was also implemented to record the panel deformations during air blast. The air and underwater blast tests represent two different regimes of blast loading: one far-field in air and one near-field underwater. The difference in deflection development, caused by the differing fluid mediums and stand-off distances, is apparent from the full-field results. During underwater blast the panel underwent peak pressure loading of approximately 52.6 MPa whilst during air blast the panel was subjected to 67.7 kPa followed by 68.9 kPa peak pressure loads in succession. The two experiments demonstrate the response of the same hybrid composite sandwich panel under two differing blast regimes.

The post-blast damage and strength of the hybrid panels following air and underwater blasts were evaluated. Post-blast testing revealed that the underwater blast causes significantly more damage compared to air blast, particularly debonding between the skins and core. The air blast panel sustains no visible rear skin/core debonding, whereas 13 regions of rear-face debonds are identified on the underwater blast panel. Sustaining no front-skin breakage was advantageous for retaining a high proportion of the compressive modulus for this hybrid layup following underwater blast. Damage mechanisms were interrelated. Determining the most detrimental type is not straightforward in real explosive and non-idealised experiments, however debonding was understandably shown to be significant. A further study to isolate failure modes and improve in situ instrumentation is ongoing.

* Corresponding author.
E-mail address: hari.arora@swansea.ac.uk (H. Arora).

Peer review under responsibility of Editorial Board of International Journal of Lightweight Materials and Manufacture.

https://doi.org/10.1016/j.ijlmm.2020.06.003

1. Introduction

Due to the complexity and cost, large-scale explosive underwater blast testing is performed infrequently. However, underwater blast loading is a complex phenomenon of significant importance to the naval industry. Due to the increasing use of composite sandwich structures in the marine, naval and other industries, the behaviour of composites during underwater blast needs to be well-characterised to prevent potentially devastating consequences in service.

Hayman details early research into instrumented large-scale underwater blast experiments [1]. Over 50 experiments were carried out by Det Norske Veritas (DNV) and the Royal Norwegian Navy to investigate composite sandwich panels with glass-fibre skins and polyvinyl chloride (PVC) foam cores. Data was gathered using 12 strain gauge channels. More recently, Arora and Kelly have performed large-scale underwater blast tests adopting a similar setup. Up to 28 strain gauges were used to monitor the panel behaviour in these experiments [2,3]. Arora compared the underwater blast performance of composite sandwich structures with woven glass-fibre reinforced polymer (GFRP) skins to structures with hybridised woven GFRP and aramid-fibre skins [2]. Both panel types had a styrene acrylonitrile (SAN) foam core. The hybridised glass-fibre and aramid-fibre panels were found to suffer greater damage. The presence of the aramid-fibres lowered the overall strength and stiffness of the panel but significant scope for optimisation of hybrids remains, given subsequent promising efforts during air-blast experimentation [4–6]. Kelly compared the underwater blast performance of sandwich panels with continuous fibre GFRP and carbon-fibre reinforced polymer (CFRP) skins, both with single density core and graded density core [3]. The high stiffness of carbon-fibre caused the panels with CFRP skins to suffer from extensive damage, especially the panels with a single density core [7]. These two experiments highlight that the intermediate stiffness of glass-fibre skins is beneficial during underwater blast loading.

Laboratory techniques have been developed to simulate underwater blast loading. The laboratory-based simulations often enable improved instrumentation techniques to be implemented. Researchers [8–10] have created an underwater pressure load by impacting a water piston with a flyer plate launched by a gas gun (sometimes referred to as a water hammer method). Latourte et al. used this method to compare the performance of GFRP composite laminates and composite sandwich panels with GFRP skins and PVC foam core [8]. The setup enabled deflection versus time recordings to be made using high-speed photography and the shadow Moiré technique. Sandwich panels were shown to outperform laminate panels at high specific impulses. LeBlanc et al. [11,12] have used a conical shock tube (CST) to investigate scaled-down underwater blast on composite sandwich panels. The CST is a water filled tube with conical internal shape. The underwater shock wave is initiated by an explosive at the narrow open end of the tube. The initial experiment relied on strain gauge data to record panel response [11], however, the experimental setup was further developed and transient plate response was recorded using 3D digital image correlation (DIC) [12]. High-speed cameras were positioned behind the back face of the composite sandwich panel. This experiment investigated the effect that polyurea coatings have on composite sandwich panels with GFRP skins. The authors found that for a given polyurea thickness, the panels demonstrated greatest resistance to deformation for a given blast when the coating was applied to the back skin.

These research papers demonstrate that polymer coatings and hybrid composites could prove beneficial during underwater blast loading, if an optimal trade-off between strength and stiffness can be achieved. Extensions of such methods from blast simulators to real explosive charges in water tanks has enabled full-field measurements to be performed on small charges (<1 g) [13]. The structural response that occurs between blast wave arrival and full panel deflection has not been captured photographically during a large-scale underwater blast experiment. The research presented in this paper seeks to investigate whether a hybrid composite sandwich panel, using GFRP and CFRP, achieves good blast resilience and demonstrates how the deflection of the panel can be captured using high-speed 3D DIC. This study enables a comparison between air and underwater blast performance to further characterise the dynamic behaviour of this hybrid composite sandwich structure.

2. Experimental methods

2.1. Materials

The hybrid sandwich composite panel was 1.39 m × 1.23 m in size and was constructed from four layers of bi-axial stitched fabric either side of a 30 mm thick Divinycell H100 PVC foam core. The fabric layers were arranged quadriaxially and were infused with SR8100 epoxy resin and SD8824 hardener. The panel was fabricated using resin infusion and was ambient cured and then held under vacuum for 24 h before being demoulded. A schematic diagram, showing the layup of the hybrid panel, is shown in Fig. 1. This hybrid panel layup was selected based on results from existing research. Previous underwater blast testing has demonstrated the disadvantages of using CFRP skins during localised underwater blast due to their brittle behaviour which leads to greater damage and failure compared to CFRP skins [7]. It was desired to investigate whether the inclusion of a small proportion of carbon-fibre within a majority glass-fibre skin could improve panel strength yet result in acceptable levels of damage. This hypothesis has been investigated for air blast and high velocity impact [6,14]. The results from these experiments demonstrated the benefits of adopting an asymmetric sandwich panel, if loading direction was known. Furthermore, a dispersed hybrid skin was shown to be effective under impact loading [14]. The layup configuration shown in Fig. 1 was selected as it implements the recommendations from these investigations. Table 1 details the mechanical properties of the materials which were used to calculate panel properties detailed in Fig. 1.

2.2. Underwater blast experimental method

All blast experiments in this article were conducted at Radnor Range Ltd., Presteigne, UK. The test panel was mounted onto one side of a steel cubicle. The panel was bolted to the cubicle along the top and bottom edges using 8 × M12 bolts and clamped to the cubicle along the vertical edges. The panel and steel cubicle overlapped by 100 mm to enable the bolting and clamping fixing methods. A 5 mm thick steel frame was placed up against the panel to help distribute the bolting and clamping forces. In addition, a custom made epalyn rubber, box welded pond liner was adhered to the inside of the steel frame using Sikaflex 291i marine sealing adhesive and Loctite 406. This created a water-tight seal when the frame was tightened up against the panel using the bolts and clamps. An enclosure for the body of water was created from pendine concrete blocks. This block enclosure had the same dimensions as the pond liner and provided support for the liner when filled with water. A photograph of the test setup under construction is shown in Fig. 2. Water was pumped into the enclosure to a depth of 1525 mm. A 1 kg spherical PE7 charge was placed at a depth of 275 mm, in line with the panel centre point, and at 1 m stand-off

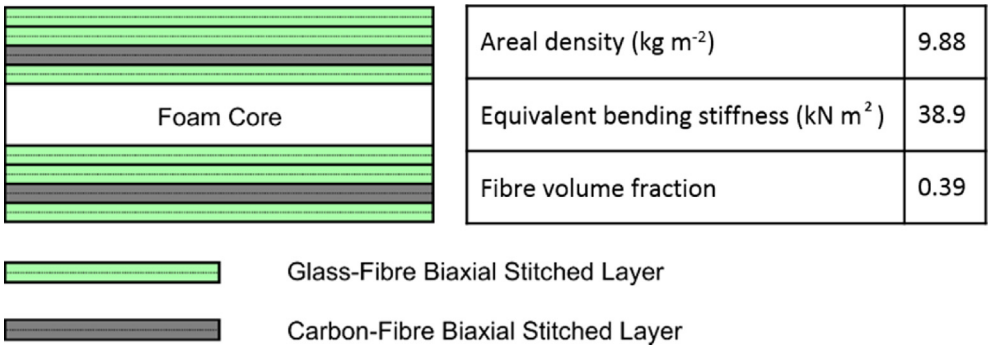

Fig. 1. Layup configuration of the hybrid composite sandwich panel subjected to underwater blast testing. The top of the diagram corresponds to panel front.

Table 1
Properties of the composite sandwich panel materials.

Material	Density (kg m^{-2})	Elastic modulus (GPa)	Tensile strength (MPa)	Compressive strength (MPa)
Glass-fibres	2555	78.5	2000.0	4500.0
Carbon-fibres (HexTowAS4)	1790	230.0	4410.0	4950.0
SR8100 epoxy & SD8824 hardener	1119	2.7	50.0	103.0
PVC H100 foam core	100	0.1	3.0	2.7

distance from the panel. To simulate a partially submerged naval vessel being subjected to a small, near-field mine explosion, 70% of the panel was submerged and the remaining 420 mm was above the water level. A schematic diagram showing the test setup is shown in Fig. 3. Although this setup is highly bespoke, it aims to demonstrate the feasibility for the measurement and the variability of outcomes that can be expected due to factors such as mine proximity and impact depth. Due to financial constraints the experiment was limited to a single shot with this setup, enough to prove the concept for future experiments.

The variation of pressure with time for an underwater shock wave is given in Equation (1), where $P(t)$ is the pressure acting at time t, P_m is the maximum overpressure at the shock wavefront and θ is the time constant for $P(t)$ to fall to P_m/e. It is possible to calculate P_m from empirically derived equations expressed in terms of scaled distance, such as Equation (2) [15]. Here Z is the scaled distance, given in Equation (3), where R is stand-off distance from charge in metres and W is weight of charge equivalent to TNT in kg. Using Equation (1), the expected pressure loading above atmospheric on the panel for the experimental setup detailed was 52.63 MPa (with an expected duration of approximately 0.5 ms based on previous experiments in shallow water [3]). However, given proximity to the free-surface, target and boundaries this is likely to differ. Numerical methods are well suited to determine the exact loading differential across the target face, but these empirical equations give reasonable estimates.

$$P(t) = P_m exp\left(\frac{-t}{\theta}\right) \tag{1}$$

$$P_m = \frac{355}{Z} + \frac{115}{Z^2} - \frac{2.44}{Z^3} \tag{2}$$

$$Z = \frac{R}{W^{1/3}} \tag{3}$$

Fig. 2. Photograph showing cubicle and pendine concrete block setup for underwater experiment whilst under construction.

3D DIC was implemented to capture the full-field response of the panel during underwater blast loading. A pair of Photron SAX2s recording at 12,500 fps were placed behind the panel. The cameras were triggered via a manual switch at the same time as the charge detonation switch. The cameras were housed within the test cubicle and mounted horizontally on an aluminium extrude bar attached to a heavy-duty camera stand. Horizontal mounting was preferred here as a safety precaution to avoid camera submersion in case of an unexpected catastrophic sample failure and flood occurrence. Precautions relating to electrical cable isolation from a potential water breach were also taken. 24 mm lenses were used on all cameras to ensure the panels were within the field of view (FOV). Banks of LED lights were used to illuminate the back skin of the panels during blast testing. Calibration of the cameras was carried out using a 700 mm CC coded calibration cross supplied by GOM UK. A speckle pattern was painted on the back skin of each panel to facilitate DIC. The rear skin of the panel was painted matt white and a random black speckle pattern was applied to enable DIC processing. A photograph of the camera setup within the cubicle, along with the panel speckle pattern is shown in Fig. 4. An additional high-speed Photron SA1 camera was setup to record the detonation event and its effects within the test arena. This camera was mounted on the bank of the test arena, recording at a frame rate of 2000 fps.

2.3. Air blast experimental method

An identical hybrid composite sandwich panel was subjected to repeated large-scale air blast testing, two 8 kg charges in

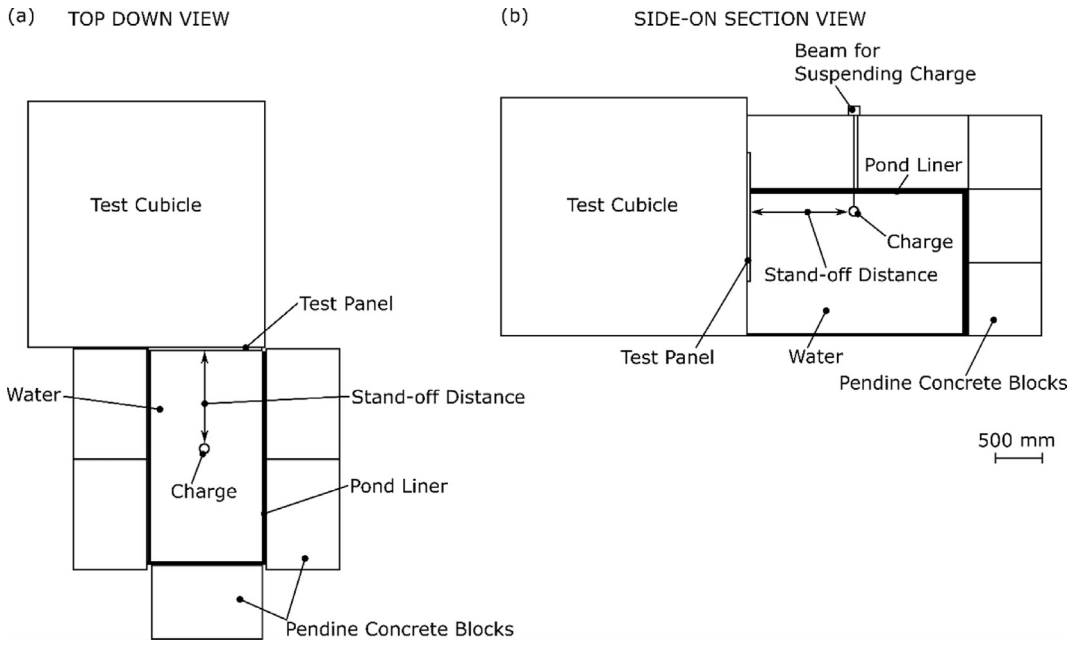

Fig. 3. Schematic diagram of the test setup showing: (a) view of setup from above and (b) side-on section view of setup.

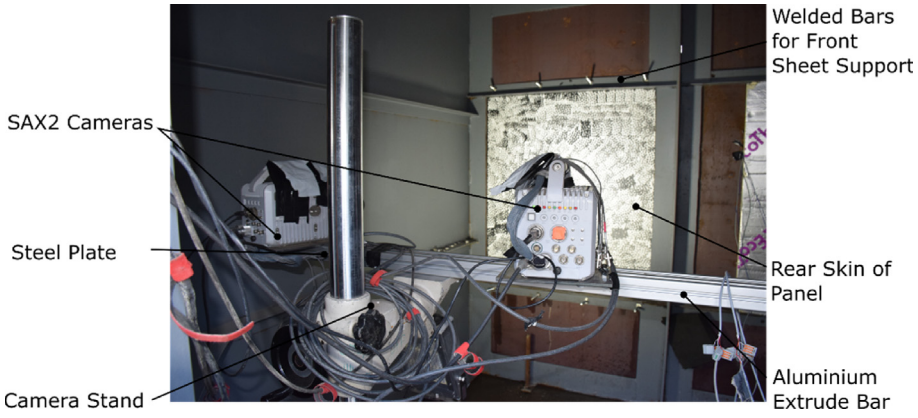

Fig. 4. Photograph showing the camera setup during the underwater blast experiment.

succession. The hybrid panel was the same size: 1.39 m × 1.23 m, and was constructed at the same time as the underwater blast panel with the same materials. The panel was mounted onto one side of the steel cubicle using the same fixing method as the underwater blast experiment. The panel was bolted to the cubicle along the top and bottom edges using 8 × M12 bolts and clamped to the cubicle along the vertical edges. A 5 mm thick steel frame was placed up against the panel to distribute the bolting and clamping forces. An 8 kg PE7 charge was placed at 8 m distance perpendicular to the panel. The charge was raised to the centre height of the panel by placing it on polystyrene which, in turn, was placed on a steel plate to prevent ground cratering. The panel was subjected to two 8 kg PE7 charges at 8 m stand-off in succession. This would result in more significant panel damage which would be more comparable to the post-blast damage caused by a single underwater blast. A photograph of the front of the test cubicle and one of the charge and side-on pressure gauge for the air blast experiment are shown in Fig. 5. Pendine concrete blocks were positioned to the side of the test cubicle to minimise blast clearing around the panel, creating a more uniform pressure load across the panel front. The cubicle height was extended vertically to prevent the same blast clearing effect over the top of the cubicle.

A side-on pressure gauge was positioned 8 m from the charge, placed perpendicular to the path of the blast wave to measure static overpressure. 3D DIC was implemented to capture the response of the panel rear face during air blast loading. The same setup as detailed in Section 2.2 was used. However, the cameras recorded at a reduced frame rate of 4000 fps, due to the expected longer panel response time, whilst maximising spatial resolution.

The side-on overpressure, P_{so}, during an air blast can be calculated from an empirically derived equation expressed in terms of scaled distance, detailed in Equation (4) [15]. This can be converted to estimate reflected overpressure, assuming the blast wave and target panel are perpendicular, using Equation (5) [15]. Here P_r is reflected overpressure and P_0 is ambient pressure. Using Equations (4) and (5), the expected side-on overpressure was 58.2 kPa and reflected overpressure was 151.8 kPa for the air blast setup. The reflected overpressure experiences by the panel under these experimental air blast conditions is over 300 times lower than for

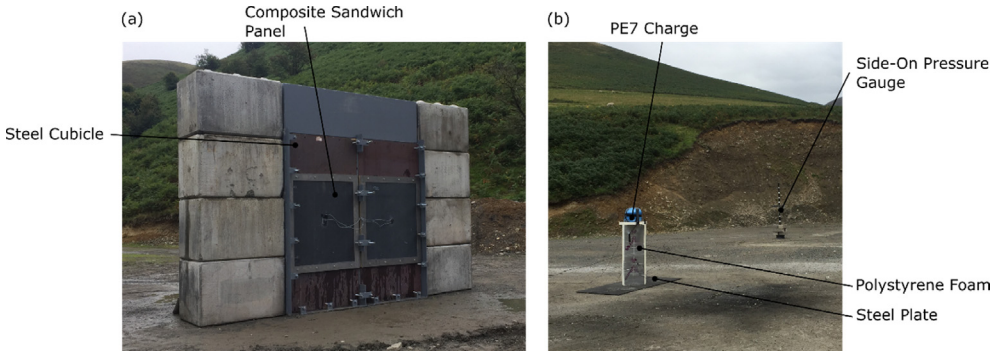

Fig. 5. Photographs showing: (a) cubicle setup for air blast experiment and (b) charge and side-on pressure gauge.

the underwater blast conditions. The underwater blast peak pressure is significantly higher due to the closer proximity of the charge to the panel in the underwater blast setup and due to the increased density of water relative to air.

$$P_{so} = \frac{108}{Z} - \frac{114}{Z^2} + \frac{1772}{Z^3} \tag{4}$$

$$P_r = 2P_{so}\frac{4P_{so} + 7P_0}{P_{so} + 7P_0} \tag{5}$$

2.4. Post-blast damage assessment method

Following blast testing, the damage sustained by the hybrid panels was recorded and evaluated. Both panels were sectioned, and all edges were photographed and visually inspected for core cracks, front skin/core debonding and rear skin/core debonding. The damage mechanism types and severity/extent of damage was recorded. Following this, 300 mm × 200 mm specimens were taken from the panel and subjected to edgewise compression loading. These compression specimens were taken from various locations across the panels and had sustained varying amounts of visibly-observable damage during the blast test. Compression testing was performed to simulate the structural loads experienced by the panels during service, furthermore, the compressive strength of composite laminates is considerably lower than their tensile strength. Therefore, compressive strength is usually the critical design criteria. Testing was performed using an Instron 5985 universal testing machine at a quasi-static test rate of 2 mm min^{-1}. A Nikon D7100 DSLR camera was used to capture one photograph every second to measure the strain using 2D DIC. A speckle pattern was painted on one side of each specimen to facilitate DIC. Due to the size and orientation of the specimen, out of plane displacement was not expected to occur enabling the use of 2D DIC. To ensure even loading, 10 mm thick rubber spacers were placed between the machine platens and the steel plates. 2D DIC was adopted due to potential slipping at the platens resulting in inaccurate machine displacement readings. An effective edgewise stiffness was calculated from the in-plane engineering stress and average strain. The damage types, extent of damage and post-blast properties, caused by the differing blast test methods, were compared.

3. Results

3.1. Underwater blast results

The progression of the underwater blast is shown in Fig. 6, providing an external overview of the event. The images show the detonation of the charge and a column of water travelling upwards from the water surface. A series of images illustrating the back-skin deflection and major strain at approximately 0.5 ms time intervals are shown in Fig. 7. The images in Fig. 7 (a) show an initial out-of-plane deflection of the panel. During this phase, the panel deflects to a maximum of 90.4 mm and experiences maximum major strain 1.34%. The deflection of the horizontal cross-section at the centre of the panel at intervals of time is shown in Fig. 7 (b). The panel initially responds by adopting a parabolic deflection profile before the deflection changes to a typically observed “bathtub” profile. The sharp gradient discontinuities at approximately 200 mm and 900 mm across the panel width illustrate that damage to the foam core and composite laminate skins has occurred at these locations.

The first phase is followed by a short rebound of the panel, shown in Fig. 7 (c) and (d). This secondary phase of movement can be due to surface cavitation, gas bubble and water motion [16]. The panel deflection remains positive overall throughout this phase. In Fig. 7 (e) the panel experiences a second panel deflection between 42.7 ms and its maximum at 51.5 ms. Fig. 7 (f) shows the steep deflection profile at the panel edges and sharp gradient discontinuities at around 200 mm and 900 mm across the panel width result in areas of high major strain. The maximum displacement of the panel in the third phase is approximately 125 mm and major strain 1.46%. This magnitude falls in-line with strains previously reported in similar experiments, where full-field measurements could not be implemented [2,3]. The panel continues to deflect beyond 47.2 ms and remains permanently deformed. Rigid body motion compensation (RBMC) has been implemented in all DIC data to remove the movement of the cubicle and fixing system; this isolates the panel response relative to its boundaries. This deformation profile development, of parabolic shape followed by shear failure towards the supports, largely agrees with previous observations during air blast studies [17]. However, it differs from the deformation phases proposed by Hoo Fatt and Palla during blast loading [18]. These authors propose the “bathtub” shape occurs prior to the parabolic profile, which is opposite to the experimental observations shown in Fig. 7. This difference may be attributed to the partial submersion of the panel, near-field loading condition here and significant fluid-structure interaction effects. There are indications of an initial flat region moving but given the asymmetry of the water support condition and the pressure distribution across the panel surface, this soon adopts a more parabolic curvature in this axis prior to the “bathtub” profile. Later, the opposing axis highlights considerable asymmetries in deformation profile (Fig. 8).

In all image series, the lower portion of the panel experiences a greater deflection and strain compared to the upper portion. This is due to the influence of water depth. When an underwater shock wave reaches the water surface, rarefaction occurs, and the water pressure drops (blast pressure cut-off). This results in a near surface

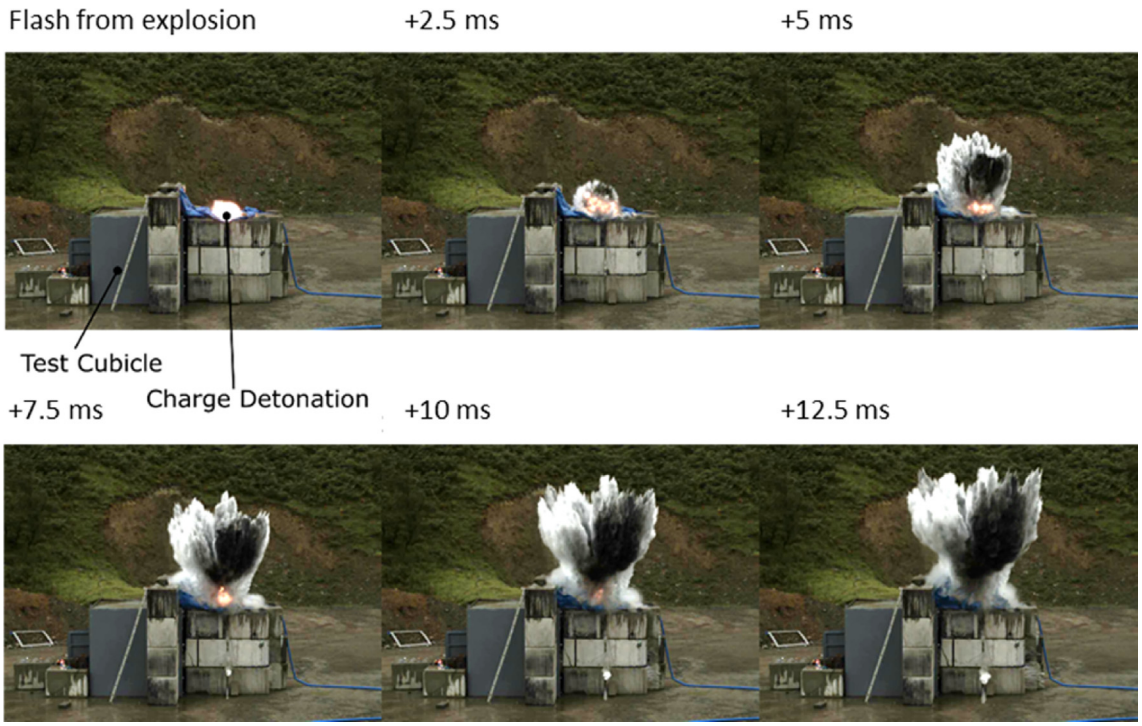

Fig. 6. Photographs of the charge detonation and progression of the water column in 2.5 ms intervals.

target experiencing a lower impulse loading compared to a submerged target. Additionally, the hydrostatic pressure of the water increases with water depth. Even without the detonation of an explosive charge, the deepest point of the panel experiences 9.5 kPa greater pressure than the point at the water surface. The detonation of a charge in this body of water, and hence the introduction of a high-pressure wave, is likely to increase this pressure difference. Lastly, the water at the base of the enclosure is confined and is unable to vent away unlike at the surface. All of these effects will result in a variation of loading with panel depth; which are complexities and real concerns for in service blast loads experienced due to surface or near-surface mines.

Fig. 8 shows the deflection of the vertical cross-section at the centre of the panel at intervals of time. This cross-section clearly illustrates the greater deflection of the lower portion of the panel. The deflection of the lowest 150 mm of the panel was not captured as the deformation profile of the panel obstructed this area from the cameras' line of sight. As highlighted earlier, vertical arrangement may be preferred to enable a few more data points to be captured but to be safe (mitigating risks relating to flooding), a horizontal was chosen as a suitable arrangement. From Fig. 8 (a), the deflection curves show that the panel beneath the surface of the water experiences deflection before the panel above the water surface responds. Fig. 8 (b) and (c) show that the deformation profile of the panel becomes linear and then curved with increasing time up to maximum deflection at 51.5 ms.

Fig. 9 shows a displacement versus time plot for the central point. The three phases of movement can be clearly seen. These phases have been labelled to correspond with the other DIC data shown in Figs. 7 and 8. There is an initial deflection to 90.4 mm, followed by a small rebound to 75.6 mm. The panel then continues to deflect and remains permanently deformed to around 125 mm. Beyond 51 ms after detonation the data becomes significantly noisy. This is due to vibrations from the ground caused by the charge and subsequent movement of the cubicle and pendine blocks. This affects the cameras and causes them to move relative to their initial positions. Fig. 9 also shows the velocity of the centre point between 30 ms and 35 ms after charge detonation. After 35 ms the noise in the displacement trace results in significant noise in the calculated centre point velocity. Despite this, the peak velocity of the panel is captured at 30.7 ms and is 44.6 m s^{-1}.

Due to the complex nature of the field experiment, the underwater pressure gauges failed to trigger during the experiment. Since no pressure data was recorded, Equation (6) was used to determine the time at which the underwater shock wave would reach the panel front using the pressure prediction from Section 2.2. This was carried out to verify whether the DIC time signatures were correct. In Equation (6), u is the particle velocity in the water, ρ_w is water density, which is assumed to be 997 kg m^{-3}, and c_w is the speed of sound in water, which is approximately 1400 m s^{-1}. By dividing the known distance between the charge and panel front by the water particle velocity calculated using this equation, the underwater shock wave is expected to reach the panel from 26.5 ms after detonation. This assumes exact positioning of the charge and ideal conditions. According to DIC data, the panel begins to deflect 30.4 ms after detonation. This correlates well with the pressure prediction, as conditions were real and not ideal, and the panel will require time to respond. Since no pressure data was recorded, it was not possible to calculate the underwater blast impulse as the decay rate was unknown. Numerical modelling of these setups is under development to shed more light on underwater blast loading characteristics.

$$u = \frac{P(t)}{\rho_w c_w} \tag{6}$$

The initial panel deflection is caused by the underwater blast wave, whilst the second panel deflection is most likely caused by shock wave reflections off the pendine blocks. Gas bubble formation is a typical underwater phenomena, which is known to cause

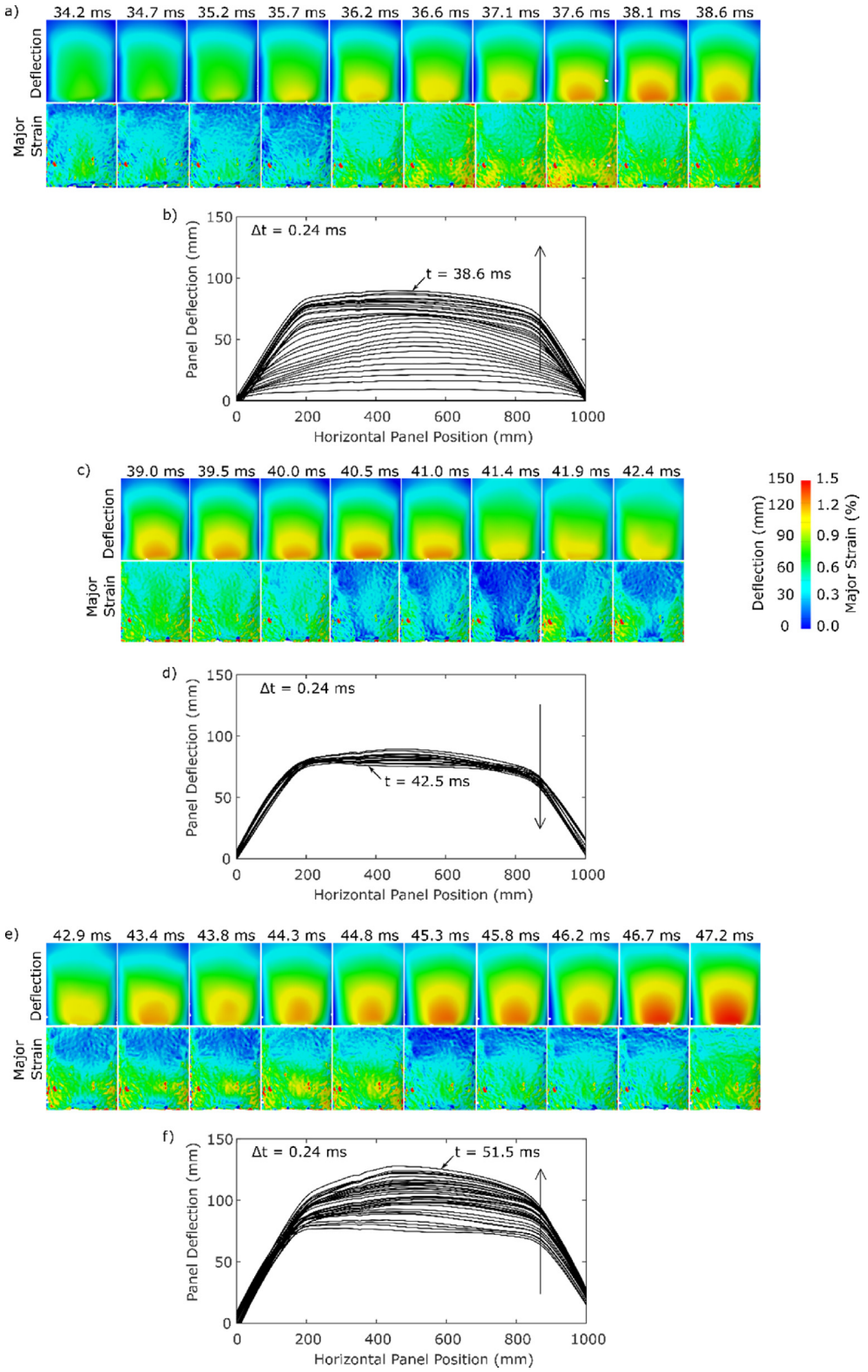

Fig. 7. DIC results for the hybrid panel during underwater blast showing: (a) initial out-of-plane displacement and major strain images, (b) deflection at time intervals for the horizontal centre section, (c) second out-of-plane displacement and major strain images, (d) rebound at time intervals for the horizontal centre section, (e) third image series and (f) repeat deflection at time intervals for horizontal centre section.

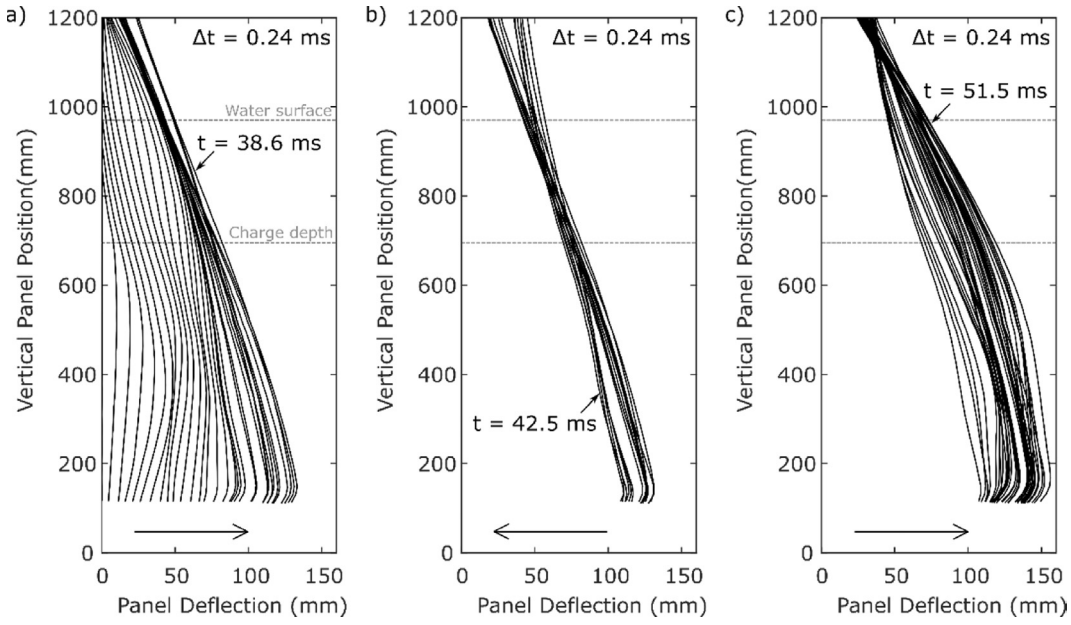

Fig. 8. DIC results for the vertical centre cross-section at intervals of time showing: (a) initial outward deflection, (b) short rebound and (c) second outward deflection.

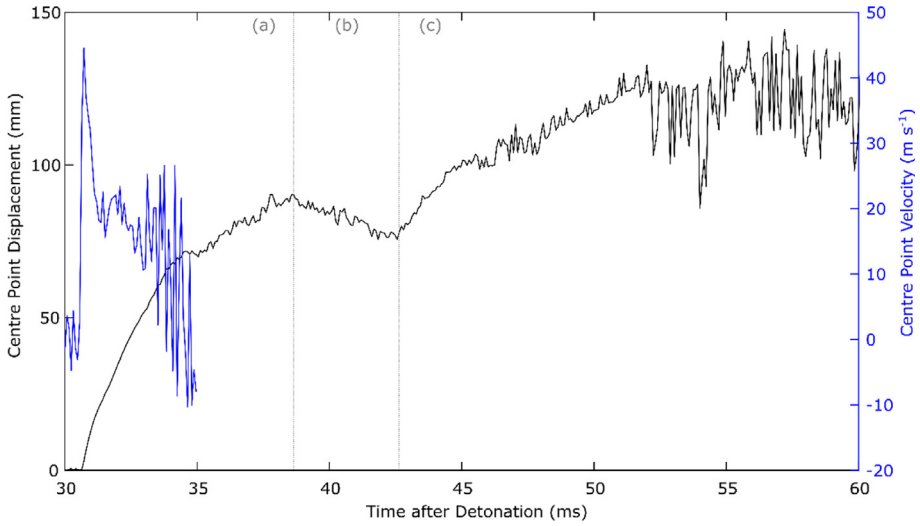

Fig. 9. Central point out-of-plane displacement against time during underwater blast loading with calculated central point velocity against time.

secondary loading of a target during underwater blast. The time period for gas bubble loading to occur under these setup conditions was calculated using Equation (7) taken from Refs. [19]. K is a constant characteristic of the explosive type and shape taken here to be 2.11 s $m^{5/6}kg^{-1/3}$ and d is the charge depth in metres. The time period of the gas bubble loading was found to equal 123 ms which does not correspond with the time at which panel second deflection occurs. Furthermore, the formation of a stable gas bubble is unlikely to occur given the proximity of the charge to the walls and free surface. Instead there is likely to be a combination of cavitation and inertial effects contributing towards this secondary loading cycle.

$$T = \frac{KW^{1/3}}{(d+33)^{5/6}} \tag{7}$$

Using the underwater shockwave velocity calculated from Equation (6), the time taken for the shockwave to reach the panel following perfect reflection of the rear wall of the pendine block enclosure and from the side walls of the enclosure were calculated. The second panel deflection lies between these two idealised shockwave arrival times indicating that various reflections at different angles off the pendine block enclosure, cavitation and inertial movement of the water are the most likely cause for the second panel deflection.

3.2. Air blast results

Fig. 10 illustrates the response of the hybrid composite sandwich panel to the first 8 kg PE7 air blast load. The panel experiences a peak central deflection of 51.9 mm and major strain of 0.78%. Panel deceleration can be seen in the return stroke along with a minor gradient discontinuity at approximately 350 mm across the panel. The deformation of the same panel under the second blast load is shown in Fig. 11. The deflection and strain images in Fig. 11 indicate

the location of a severe crack approximately 350 mm across the panel. The maximum central out-of-plane displacement of the panel under the second blast load was 58.0 mm and maximum central major strain was 0.77%.

The deflection for the horizontal centre cross-section, shown in Figs. 10 and 11, largely retains a parabolic profile. As mentioned, the presence of the discontinuity indicates the location of a crack within the foam core or composite laminate skins. This discontinuity, and crack, are exacerbated under the second blast load. There are no discontinuities towards the edges of the panel, unlike in the underwater blast experiment, and the panel does not form a "bathtub" deflection shape. As expected, the repeated blast load results in damage accumulation leading to lower bending stiffness, greater deflection and longer period of oscillation under the second blast.

The central vertical cross-section of the panel at intervals of time is shown in Fig. 12 for the first air blast and Fig. 13 for the second air blast experiment. The response of the panel under air blast is more symmetrical, in comparison to the response during underwater blast due to the negligible changes of hydrostatic pressure across the panel length. The centre of the panel experiences the greatest deflection while the top and bottom edges of the panel remain constrained. The cross-sectional displacement initiates with a flat central region (as suggested by Ref. [18]) and then remains parabolic for the remainder of the oscillation for both blast loads. The blast wave is impinging uniformly across the vertical panel length during air blast, unlike during underwater blast.

Fig. 14 shows the displacement and velocity of the centre point of the panel under both air blast loads. The peak side-on pressure during the first trial was 67.7 kPa and peak pressure for the second trial was 68.9 kPa. The side-on pressures recorded are greater than the value predicted by the empirical formula which was 58.22 kPa. The increase in displacement between the first and second trials can be clearly seen. The response period for the panel increases between the first and second blast. This is likely due to the greater damage present during the second trial resulting in an elongated return. The panel displacement curves can be seen to deflect and then undergo a damped return to zero displacement. This is unlike the underwater blast where the panel underwent a second deformation cycle, suffered more significant apparent damage and remained permanently deformed. The peak centre point velocity occurring in the second air blast was 34.1 m s^{-1}. This velocity is over 10 m s^{-1} slower than the velocity reached during underwater blast. Additionally, the panel acceleration to reach this peak velocity is significantly higher during underwater blast.

3.3. Post-blast damage results

Fig. 15 (a) shows the front view of the hybrid panel following underwater blast and after sectioning, the red dashed boxes highlight the sections subjected to edgewise compression testing. The panel suffers from several skin breakages and cracks initiating from the bolt holes. Tearing through both skins and the foam core has occurred at all four of the bottom bolt holes. There are regions of front skin delamination across the panel. The DIC contour images highlight the areas of debonding and core shear cracking one-quarter and three-quarters across the width direction. Sharp changes in deflection gradient and high areas of strain are visible in these regions. Fig. 16 (a) shows the cross-sections of the hybrid panel as viewed from the bottom of the panel. The permanent dishing of the panel is visible along with extensive core shear cracking and debonding between the skins and core. It is evident that the near-field underwater blast has resulted in severe panel damage. Fig. 16 (b) highlights a cross-section at the mid-plane where shear core cracks are visible approximately 150 mm in from the panel edge along with debonding. The core shear cracks are at approximately 45° to the through thickness direction. Front skin debonding propagates towards the panel centre and rear skin debonding towards the panel edge. The dished shape of this section can also be clearly seen. Fig. 15 (b) shows the front view of the hybrid panel following air blast testing. The air blast panel suffers from a front skin crack travelling vertically from one bolt hole to another. This front skin damage directly correlates with the gradient discontinuity and deflection peak observed in the DIC analysis of the air blast. The cross-sections of this panel are shown in Fig. 17. Core cracks are located around 150 mm in from the panel edges. The front skin breakage and resulting foam crack travelling perpendicular to the skins through the thickness are highlighted in Fig. 17 (b). Table 2 details the visual damage assessments based on these photographs.

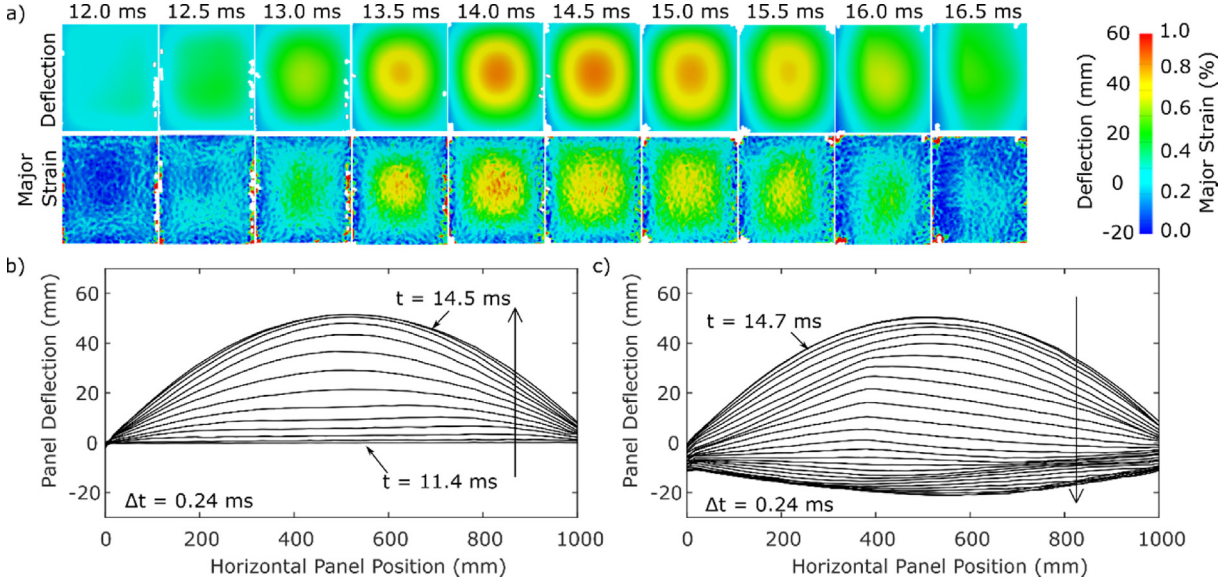

Fig. 10. DIC results for the hybrid panel under the first 8 kg PE7 charge showing: (a) out-of-plane displacement and major strain images, (b) deflection at time intervals for the horizontal centre section and (c) rebound at time intervals for the horizontal centre section.

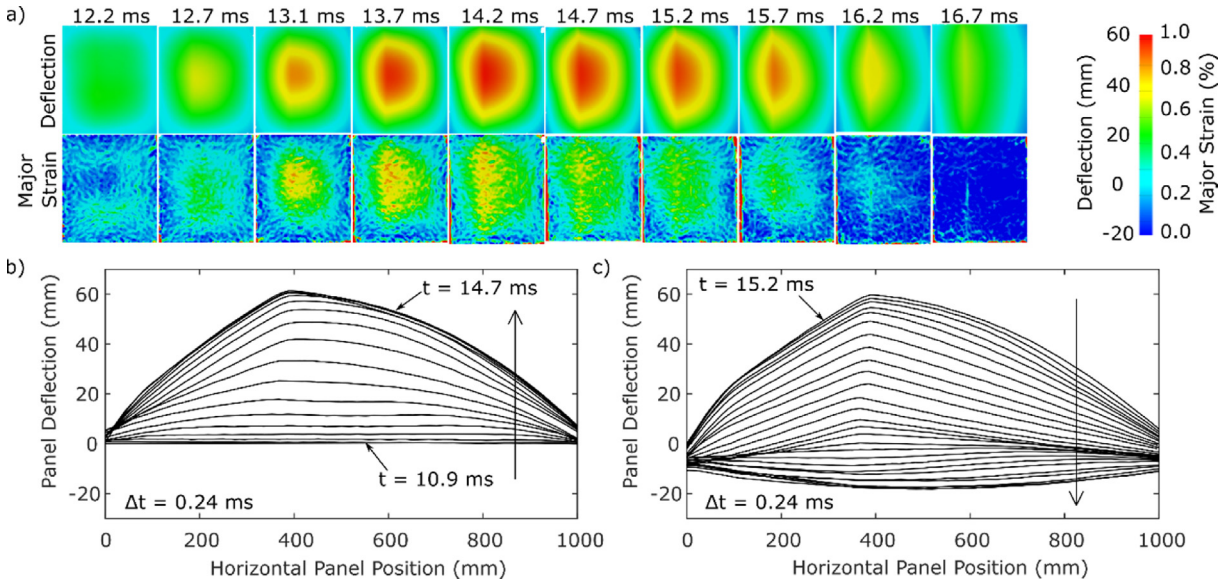

Fig. 11. DIC results for the hybrid panel under the second 8 kg PE7 charge showing: (a) out-of-plane displacement and major strain images, (b) deflection at time intervals for the horizontal centre section and (c) rebound at time intervals for the horizontal centre section.

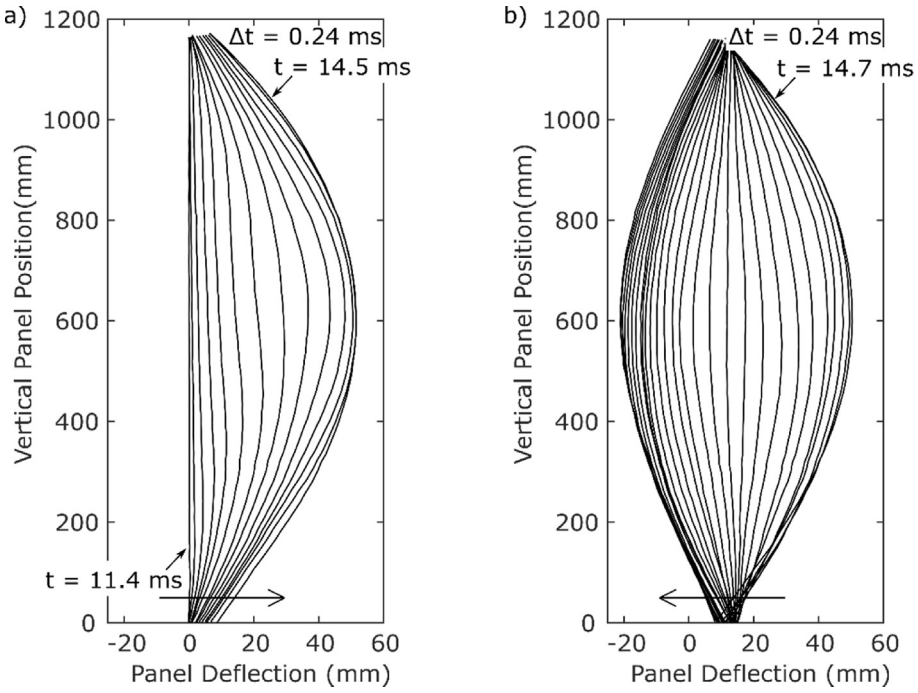

Fig. 12. DIC results for the first air blast showing: (a) deflection at time intervals and (b) rebound at time intervals for the vertical centre cross-section.

The edges and front of each 300 mm × 200 mm specimen were photographed before compression testing. This was performed to record the visual damage to the specimen using the same method as for the larger panel sections. A damage percentage was then calculated for each specimen which took front skin breakage, skin/core debonding and core shear cracks equally into account. Fig. 18 shows damage percentage versus effective compressive modulus for the hybrid panel following underwater blast loading. As damage increases, the effective modulus decreases. The graph highlights two significant outliers away from the general trend line. Specimen 4, with 23% damage and modulus of 7.7 GPa, sustained a small amount of all damage types. The low compressive modulus of this specimen could be caused by the interaction of the different damage types. Specimen 8, with modulus 28.8 GPa and 37% damage, was one of two specimens with no front skin breakage. However, regions 1, 4, 5 and 8 are expected to see the most damage given proximity to a constrained edge (as highlighted previously [2,20]), and these do seem to be visibly the most damaged regions. Skin properties dominate the compressive stiffness of the sandwich. The other specimen with no front skin breakage (number 6) demonstrated the highest effective modulus and 0% damage. This indicates that retaining an intact front skin is advantageous following an underwater blast load.

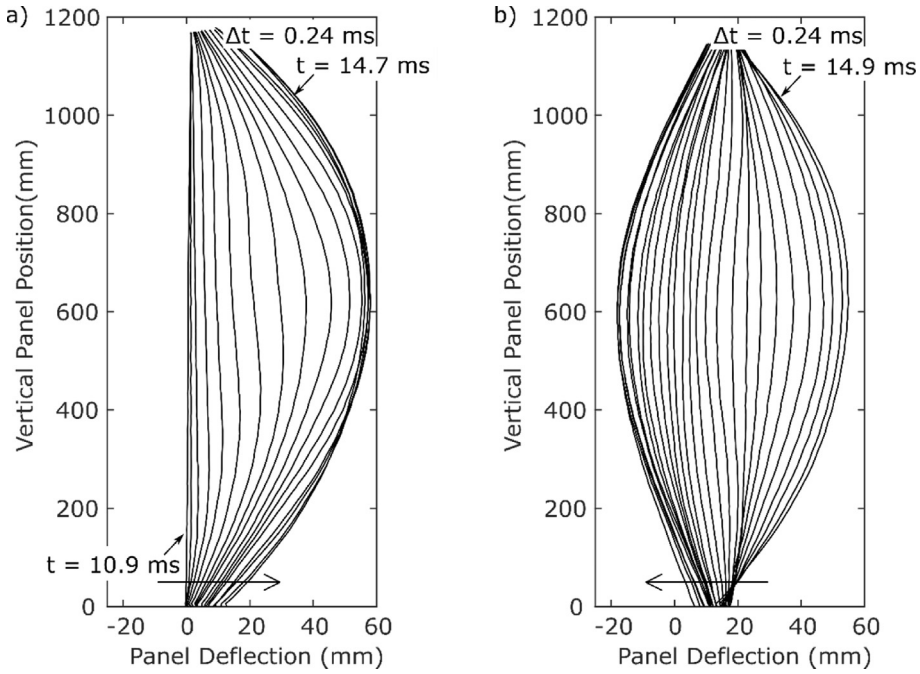

Fig. 13. DIC results for the second air blast showing: (a) deflection at time intervals and (b) rebound at time intervals for the vertical centre cross-section.

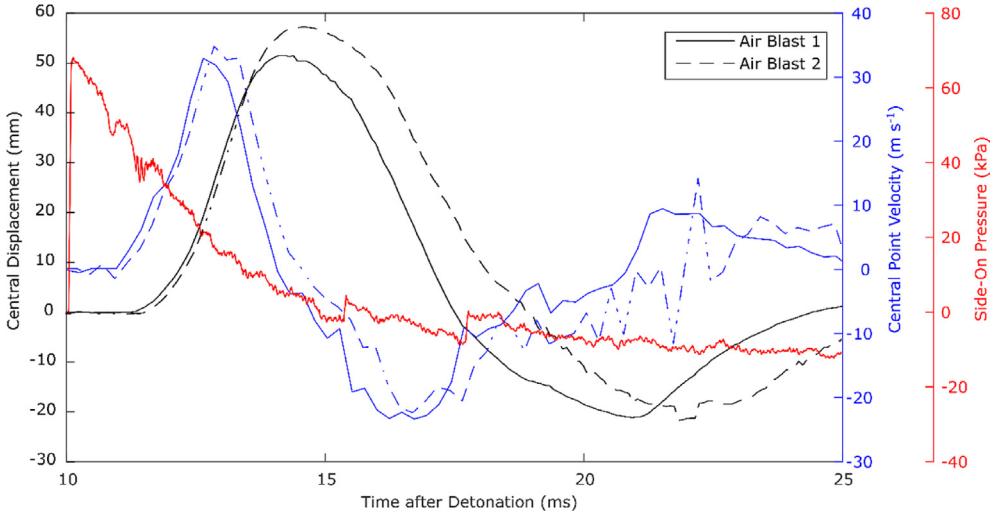

Fig. 14. Central point out-of-plane displacement against time during air blast loading with calculated central point velocity against time.

Fig. 19 plots maximum compressive stress against damage percentage. There is a trend between increasing damage and decreasing maximum compressive stress. The presence and interaction of different damage types results in four specimens lying above or below the general trend line, specimens 1, 3, 4 and 8. Research has been carried out by various authors to determine which damage mechanisms are most detrimental to post-blast strength. Kelly [3] found that debonding dominated stiffness and strength more so than core cracking. Shipsha and Zenkert [21] also showed a degradation in compressive behaviour following more intense impact load cycles, with ultimate failure coming through debonding of the skins. This is consistent with tests performed here where debonded skins proved understandably to be the weakest and that failure propagated in this manner under compression. But since the damage types were not isolated in these specimens and since the damage inspection is only visual, it is not possible to determine explicitly which damage mechanisms are causing the four outlying specimens and which mechanisms are most detrimental to post-blast compressive strength during these experiments. Further work into isolating such mechanisms is ongoing.

The post-blast compressive performance of the panels under the different load regimes can be compared, taking differing damage levels into account, to reveal some differences between air and underwater blast loading. Fig. 20 shows effective compressive modulus versus damage percentage for the two panels. The figure shows that the underwater blast causes greater panel damage ranging between 0% and 53% whereas the two 8 kg PE7 air blast loads cause damage between 0% and 21% only. This is due to the more severe regime that is created with the presence of water and reduced stand-off to the charge. There is a general trend between

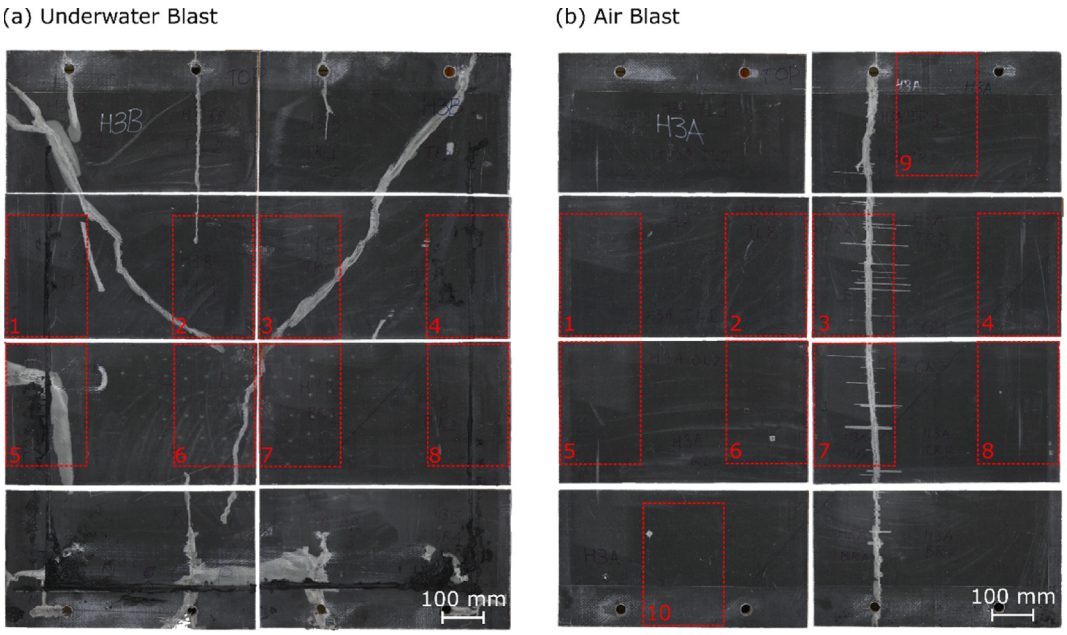

Fig. 15. Photographs showing the front of the hybrid panels following: (a) underwater blast and (b) air blast.

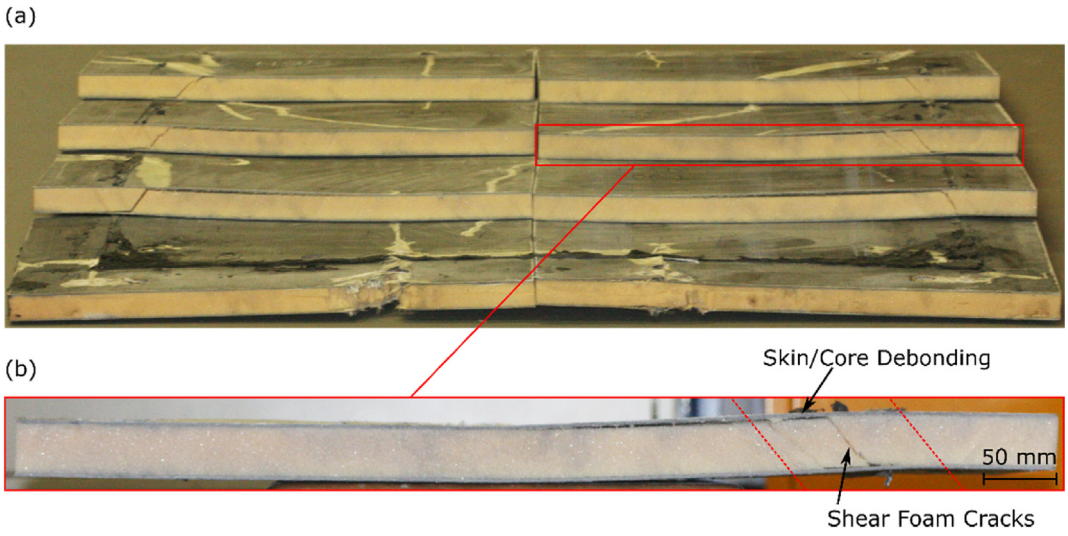

Fig. 16. Photographs showing the damage to the core and skins of the hybrid panel following underwater blast.

increasing damage percentage and decreasing effective modulus. Some specimens which achieve the same damage percentage through the two different experiments achieve a similar post-blast effective modulus, e.g. air blast specimen number 4 and underwater blast specimen number 7. However, this is not the case for all specimens. Air blast specimen 7 and underwater blast specimen 3 have a significantly different effective modulus despite achieving damage percentages of 18% and 22%, respectively. This is due to the interactions of multiple damage mechanisms which is not captured in this visual damage inspection. A significant difference between the panels occurs for the undamaged specimens. The two undamaged specimens with moduli values around 34 GPa are achieving modulus values comparable to those of damaged specimens. It could be possible that damage in these specimens is present but has not been identified visually. Detailed microstructural analysis can help to determine this but is not always feasible for large scale structures [7]. There is a significant drop in effective compressive modulus between specimens with zero damage and those with damage.

Fig. 21 shows a plot of maximum compressive stress versus damage percentage. The air blast and underwater blast panels show consistent post-blast behaviour. The specimen maximum compressive stress decreases as damage percentage increases with no significant drop following the initial onset of damage. There is a general trend between increasing damage and decreasing maximum compressive stress, however, there are significant outliers. Once again, this is due to the interactions between the damage types. Post-blast testing revealed that sustaining no front skin breakage was advantageous for retaining a high proportion of the compressive modulus of the panel following underwater blast. This is in direct contrast to the post-blast assessment results for the panel following air blast. During air blast loading, the panel suffered

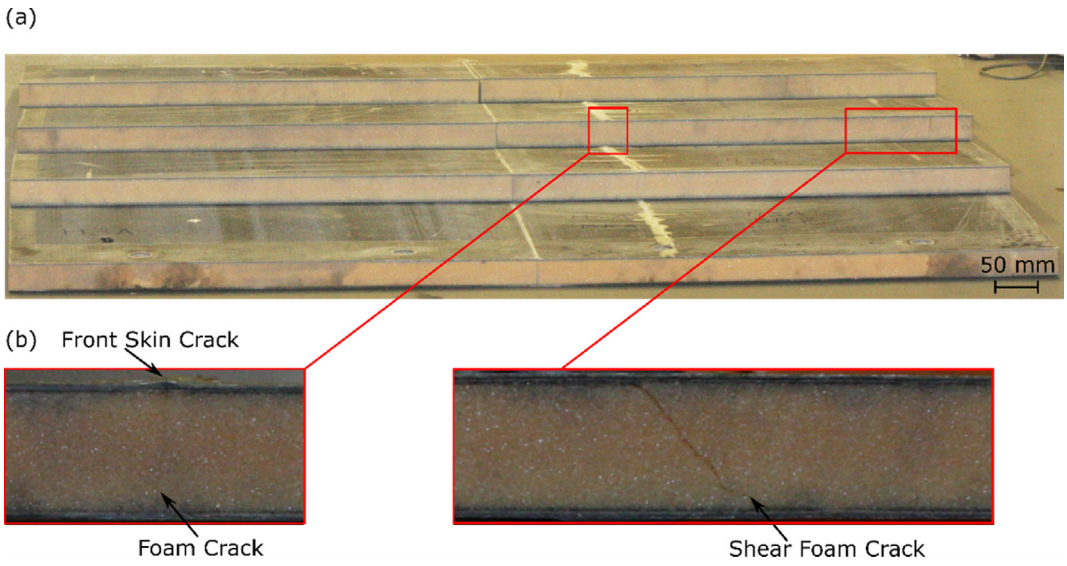

Fig. 17. Photographs showing the damage to the core and skins of the hybrid panel following air blast testing.

Table 2
Visual inspection of damage sustained by the hybrid panel following underwater blast.

Blast type	No. of core cracks	Length of core cracks (mm)	No. of core/front skin debonds	Length of front debonds (mm)	No. of core/rear skin debonds	Length of rear debonds (mm)	Length of front skin cracks (mm)
Underwater	19	808	17	2163	13	555	2993
Air	8	305	3	77	0	0	1368

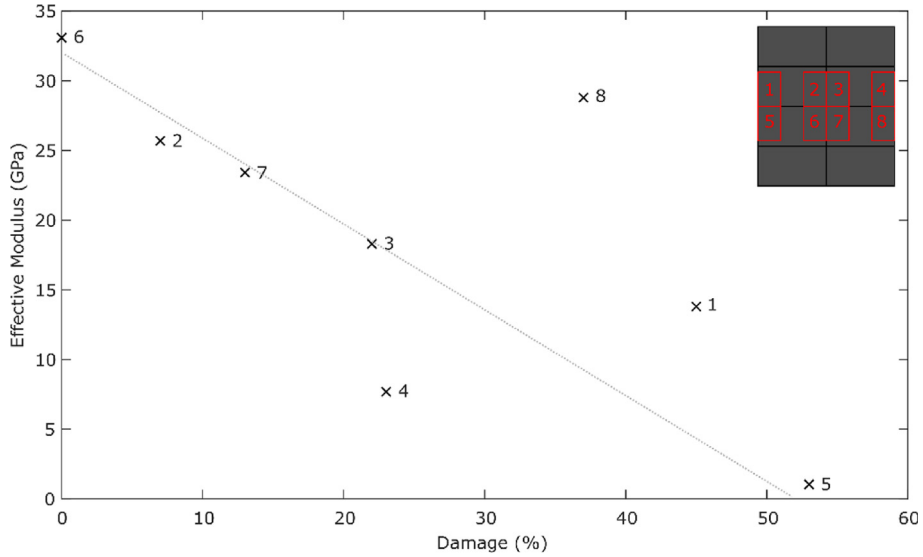

Fig. 18. Post-blast effective modulus versus damage percentage for the specimens taken from the underwater blast hybrid panel. Numbers correspond to the location labels in Fig. 16(a).

from a significant front skin and core crack yet these specimens, numbers 3 and 7, demonstrate relatively high post-blast compressive performance. These specimens which suffered from a front skin and core crack did not sustain other damage, therefore, the overall integrity of the specimen was controlled. Conversely, the underwater blast panels with front skin cracking also suffer from delamination and debonding. Therefore, the front skin damage with an interaction of multiple mechanisms reduces the strength of the specimens. Avoiding front skin damage in the underwater blast specimens would prevent these interactions and would be beneficial, as isolated front skin damage is not detrimental to post-blast compressive strength.

4. Discussion

This investigation was performed to develop an underwater blast setup with implementation of DIC to record full-field panel response. In general, the trial proved a success as full-field DIC was

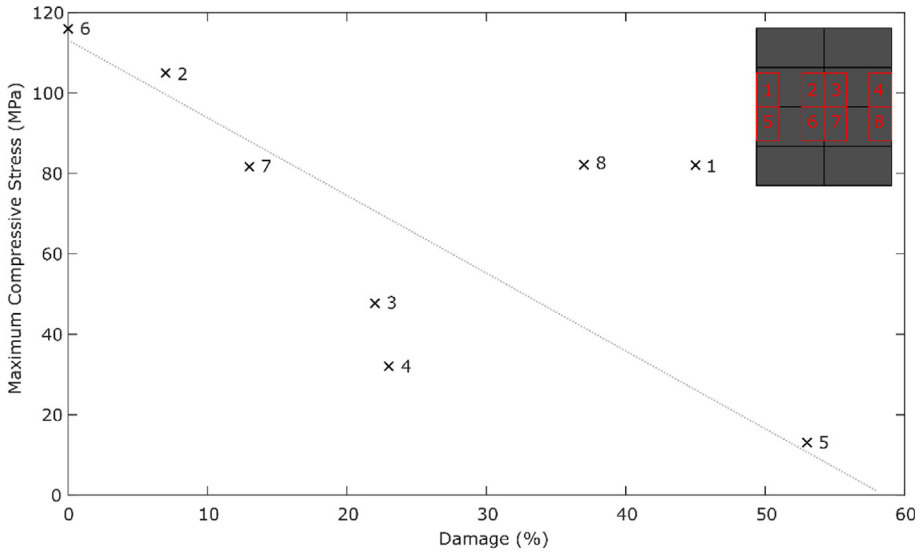

Fig. 19. Post-blast maximum compressive stress versus damage percentage for the specimens taken from the underwater blast hybrid panel. Numbers correspond to the location labels in Fig. 16(a)).

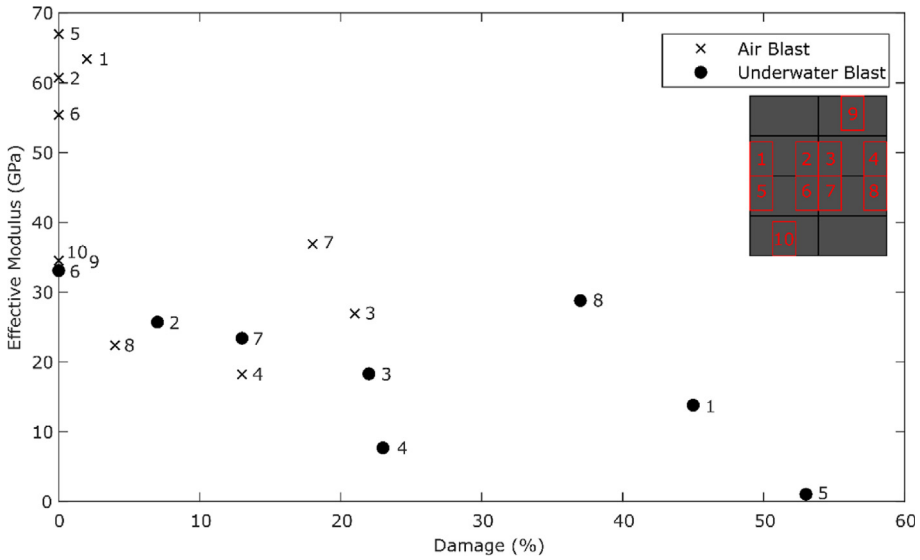

Fig. 20. Post-blast effective modulus versus damage percentage for the specimens taken from the air and underwater blast panels.

captured. The trial highlighted areas of improvement for future testing. Initial observations of the DIC data shows that the cameras successfully captured the response of a large area of the panel. The camera frame rate, which was 12,500 fps, was sufficient to capture the panel response during underwater blast.

Only one composite sandwich panel was subjected to underwater blast testing due to time and experimental constraints. This data set is too small to definitively quantify the underwater blast behaviour of hybrid composite sandwich panels. Nevertheless, the results provide an insight into key experimental observations. DIC enabled full-field rear skin deflection and strain tracking. The DIC results showed a small pulsation in panel deflection and strain during underwater blast. The panel centre point was shown to deflect to 90.4 mm then rebound slightly to 75.6 mm before deflecting again to approximately 125 mm. This pulsation is likely to be caused by shock wave reflections off the pendine concrete enclosure in which the underwater explosion occurred, given the time of flight between pulses/deformations, as well as various hydrodynamic phenomena.

The strain contour maps and deflection cross-sections highlighted that the horizontal cross-section of the panel deforms in a parabolic shape during underwater blast until excessive deflection causes core shear cracking. The panel then forms the commonly observed “bathtub” deformation shape. These areas of core cracking and core/skin debonding are regions of weakness for the panel. These damaged areas could be lessened if the mounting structure was able to undergo deflection to some extent. These results reinforce the importance of support structure design on overall blast resilience. Mouritz [22] highlights the current lack of work in the area of interfacial property optimisation for blast. Finally, the DIC results capture the response of the panel vertical cross-section. The panel section 300 mm beneath the charge experiences deflection first. Following this, the deflection profile becomes parabolic as the entire panel length experiences deflection.

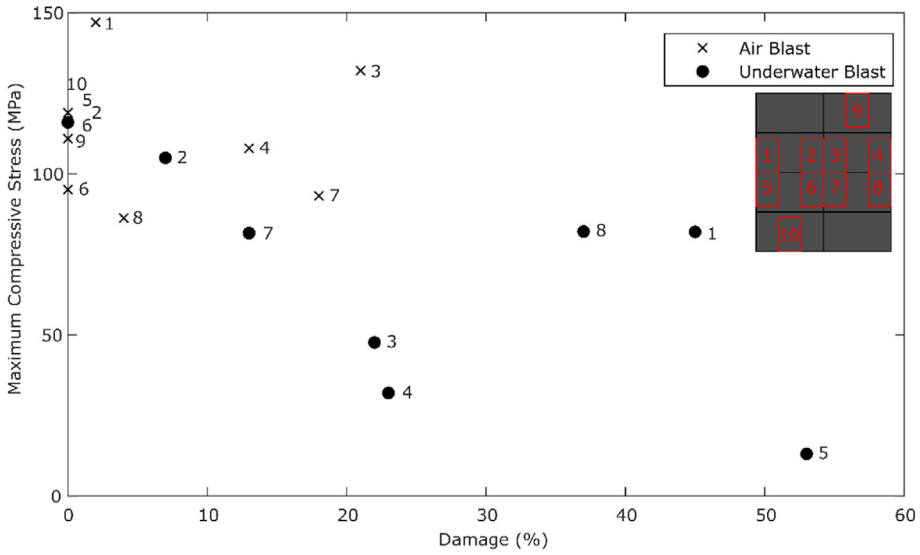

Fig. 21. Post-blast maximum compressive stress versus damage percentage for the specimen taken from the air and underwater blast panels.

The greatest point of deflection remains around 300 mm beneath the charge. Due to the presence of water more severely loading the lower portion of the panel, severe damage occurs approximately 600 mm beneath the charge depth. This weak point then experiences the greatest out-of-plane displacement.

Full-field DIC has highlighted that water depth significantly influences panel deflection, strain and hence damage sustained, as expected, due to the physical parameters of the experimental setup. The results have shown that it is incorrect to assume a symmetric response around the panel mid-plane for a large-scale panel near the water surface. This is a complex transition region for panel response and needs detailed consideration of initial condition and loading variability.

The DIC data reveals that the panel deflection remains largely parabolic throughout both air blast loads. A gradient discontinuity shows the location of a crack, later confirmed through damage inspection. However, the "bathtub" deflection shape and significant loss of panel integrity at locations one quarter and three quarters across the panel does not occur under the air blast load experienced. The vertical and horizontal cross-sections of the panel under air blast demonstrate that the blast wave is uniformly spread across the panel face and the centre point experiences the greatest deflection. This is unlike during underwater blast in which deflection was influenced by water depth (target depth, position of charge and degree of structure submersion). There is a 10 m s^{-1} difference between the peak centre point displacements reached by the panels during air and underwater blast. During underwater blast, the panel reaches a higher velocity and undergoes a far greater acceleration to the peak velocity. These observed differences are due to the significant difference in loading between the air and underwater experiments. During air blast loading, the panels experienced 68.9 kPa peak side-on pressure. This is expected to cause a calculated peak reflected overpressure of 174.4 kPa. This is over 300 times smaller than the predicted underwater blast pressure of 52.63 MPa. Although the underwater blast impulse was not captured, the panel velocities show the underwater blast panel responded in a far shorter time. With less response time available during underwater blast, the panel is unable to undergo a global response, unable to engage more of the structure/material. Therefore, more significant damage occurs in discrete locations throughout the structure, where stresses are greatest inset from the boundary, resulting in the permanently deformed "bathtub" shape. During air blast, the panel can undergo global bending and can rebound/oscillate more freely. This absorbs/dissipates blast energy resulting in less damage and hence the panel exhibits a damped oscillatory response back to zero displacement.

As detailed, the empirical air blast side-on pressure prediction was 58.22 kPa and the experimentally recorded maximum side-on pressure was 68.9 kPa. This leads to a prediction uncertainty of 15.5%. If the same uncertainty can be applied to the underwater pressure empirical prediction, the underwater pressure will lie between 44.79 MPa and 60.79 MPa. However, the effect of the water surface has not been considered in the pressure prediction. As detailed in Section 3.1, rarefaction will occur at the water surface causing a drop in pressure. This adds further uncertainty to the underwater pressure prediction and ensuring a functioning underwater pressure gauge is a key area for future experimental developments.

Post-blast visual inspection revealed significant panel damage following underwater blast. Front skin cracks, regions of debonding and through thickness tearing were identified. The panel remained permanently deformed and shear core cracks, 150 mm in from both edges running the entire panel length, were observed. As expected, significant damage occurred as a result of underwater blast testing compared to air blast testing. This is due to the increased severity of underwater blast loading compared to air. The increased density of the fluid medium gives the panel less time to respond, as highlighted by the panel response velocities, and increases the blast wave pressure by over a factor of 300. Post-blast testing revealed that sustaining no front skin breakage was advantageous for retaining a high proportion of the compressive modulus for this hybrid layup following underwater blast. This is contradictory to the results found for post air blast performance of the same hybrid panel type. However, the front skin and core crack in the air blast panel was an isolated damage type, whereas the underwater specimens suffered from front skin and core cracking along with delamination and debonding. The presence of only front skin breakage in the air blast panel was not detrimental to post-blast compressive strength (as much of the structure remained intact). Trends were observed for increasing damage and both decreasing compressive modulus and decreasing compressive strength.

Furthermore, the post-blast air and underwater compressive strength and moduli from the two panels were consistent. Since the damage types were not isolated, it was not possible to determine which damage mechanism is most detrimental to post-blast panel performance. Ref [23] highlights the need for further work in determining the relative importance of a given mitigation mechanism within a complex protective structure. Similar efforts are required in sandwich structures to maintain suitable residual strength after blast. Following underwater blast loading the compressive strength and modulus of certain panel sections fell to 13.1 MPa and 1.04 GPa, respectively.

5. Conclusions

An underwater blast experiment was conducted to demonstrate whether DIC could be successfully implemented during underwater blast testing. Furthermore, the experiment was performed to determine whether a hybrid composite sandwich panel could resist an underwater blast load. DIC data was successfully generated and the full-field response reveals more detailed results compared to previous underwater blast experiments. The pulsation of the panel, the asymmetry of the panel deflection profiles and the change in deflection profile with time have been captured during large-scale underwater blast for the first time using DIC. Due to the change in fluid medium, the strain and deflection reached by the panel during underwater blast far exceeds that reached during a typical air blast. Overall, the panel showed good blast resilience considering it withstood a pressure loading of around 50 MPa and water did not breach the panel. The post-blast modulus and strength of the air and underwater panels showed consistency. Undamaged specimen from each panel achieved similar properties. As damage percentage of the panel specimen increased, the modulus and strength consistently decreased for both panels. Underwater blast loading results in a more severe loading regime and hence more devastating damage than air blast loading. Post-blast damage inspection revealed that the samples with an intact front skin achieved a higher compressive modulus. Although only one experiment was performed in this investigation, the full-field results generated can aid in determining whether previous interpretations of strain gauge data are logical. Furthermore, this full-field data will aid in validation of numerical underwater blast models and determining whether the models are accurately recreating the underwater blast phenomenon, including influences of water depth and cross-sectional deflection.

Conflicts of interest

The authors declare that there is no conflicts of interest.

Acknowledgements

The authors would like to thank Dr Yapa Rajapakse of the Office of Naval Research [N62909-15-1-2004] for supporting Dr Emily Rolfe, Dr Mark Kelly and Dr Hari Arora during their PhDs and EPSRC for supporting Emily Rolfe. The assistance throughout the experiments from Alex Fergusson of FAC Technology, Mark Johnson of Slowmo Ltd, Amy Johnson of GOM UK and Jun Liu of Imperial College was very much appreciated. The authors would like to thank Radnor Range Ltd for the in-kind support provided for blast testing. The authors also acknowledge the support from the Sêr Cymru National Research Network Industrial Collaboration Award, which supported instrumentation costs to the project.

References

[1] B. Hayman, Underwater explosion response of sandwich structures with compliant cores, in: S. Gopalakrishnan, Y. Rajapakse (Eds.), Blast Mitig. Strateg. Mar. Compos. Sandw. Struct., Springer Singapore, Singapore, 2018, pp. 23–52, https://doi.org/10.1007/978-981-10-7170-6_2.
[2] H. Arora, P.A. Hooper, J.P. Dear, The effects of air and underwater blast on composite sandwich panels and tubular laminate structures, Exp. Mech. 52 (2012) 59–81, https://doi.org/10.1007/s11340-011-9506-z.
[3] M. Kelly, Comparing the Blast Tolerance of Different Composite Structures, Imperial College London, 2016.
[4] M. Kelly, H. Arora, a. Worley, M. Kaye, P. Del Linz, P.a. Hooper, J.P. Dear, Sandwich panel cores for blast applications: materials and graded density, Exp. Mech. (2015) 1–22, https://doi.org/10.1007/s11340-015-0058-5.
[5] H. Arora, Blast Loading of Fibre Reinforced Polymer Composite Structures, Imperial College London, 2012.
[6] E. Rolfe, R. Quinn, A. Sancho, C. Kaboglu, A. Johnson, H. Liu, P.A. Hooper, J.P. Dear, H. Arora, Blast resilience of composite sandwich panels with hybrid glass-fibre and carbon-fibre skins, Multiscale Model. Exp. Des. 1 (2018) 197–210, https://doi.org/10.1007/s41939-018-0025-9.
[7] E. Rolfe, M. Kelly, H. Arora, P.A. Hooper, J.P. Dear, Failure analysis using X-ray computed tomography of composite sandwich panels subjected to full-scale blast loading, Compos. Part B. 129 (2017) 26–40, https://doi.org/10.1016/j.compositesb.2017.07.022.
[8] F. Latourte, D. Grégoire, D. Zenkert, X. Wei, H.D. Espinosa, Failure mechanisms in composite panels subjected to underwater impulsive loads, J. Mech. Phys. Solid. 59 (2011) 1623–1646, https://doi.org/10.1016/J.JMPS.2011.04.013.
[9] V.S. Deshpande, A. Heaver, N.A. Fleck, An underwater shock simulator, Proc. R. Soc. Lond. A Math. Phys. Eng. Sci. 462 (2006) 1021–1041. http://rspa.royalsocietypublishing.org/content/462/2067/1021.abstract.
[10] A. Schiffer, V.L. Tagarielli, The response of rigid plates to blast in deep water: fluid-structure interaction experiments, Proc. R. Soc. A Math. Phys. Eng. Sci. 468 (2012) 2807–2828, https://doi.org/10.1098/rspa.2012.0076.
[11] J. LeBlanc, A. Shukla, Dynamic response and damage evolution in composite materials subjected to underwater explosive loading: an experimental and computational study, Compos. Struct. 92 (2010) 2421–2430, https://doi.org/10.1016/j.compstruct.2010.02.017.
[12] J. LeBlanc, N. Gardner, A. Shukla, Effect of polyurea coatings on the response of curved E-Glass/Vinyl ester composite panels to underwater explosive loading, Compos. B Eng. 44 (2013) 565–574, https://doi.org/10.1016/j.compositesb.2012.02.038.
[13] J. LeBlanc, C. Shillings, E. Gauch, F. Livolsi, A. Shukla, Near field underwater explosion response of polyurea coated composite plates, Exp. Mech. 56 (2016) 569–581, https://doi.org/10.1007/s11340-015-0071-8.
[14] E. Rolfe, C. Kaboglu, R. Quinn, P.A. Hooper, H. Arora, J.P. Dear, High velocity impact and blast loading of composite sandwich panels with novel carbon and glass construction, J. Dynam. Behav. Mater. 4 (3) (2018) 359–372.
[15] P.D. Smith, J.G. Hetherington, Blast and Ballistic Loading of Structures, Butterworth-Heinemann, 1994. https://books.google.co.uk/books?id=0vIeAQAAIAAJ.
[16] H. Matos, C. Javier, J. LeBlanc, A. Shukla, Underwater nearfield blast performance of hydrothermally degraded carbon–epoxy composite structures, Multiscale Model. Exp. Des. 1 (2018) 33–47, https://doi.org/10.1007/s41939-017-0004-6.
[17] S.B. Menkes, H.J. Opat, Tearing and shear failure in explosively loaded clamped beams, Exp. Mech. 13 (11) (1973) 480–486.
[18] M.S. Hoo Fatt, L. Palla, Analytical modeling of composite sandwich panels under blast loads, J. Sandw. Struct. Mater. 11 (2009) 357–380, https://doi.org/10.1177/1099636209104515.
[19] R.H. Cole, Underwater Explosions, Princeton University Press, Princeton, 1948.
[20] H. Arora, M. Kelly, A. Worley, P. Del Linz, A. Fergusson, P.A. Hooper, J.P. Dear, Compressive strength after blast of sandwich composite materials, Philos. Trans. R. Soc. Lond. A Math. Phys. Eng. Sci. 372 (2014). http://rsta.royalsocietypublishing.org/content/372/2015/20130212.abstract.
[21] A. Shipsha, D. Zenkert, Compression-after-Impact strength of sandwich panels with core crushing damage, Appl. Compos. Mater. 12 (2005) 149–164, https://doi.org/10.1007/s10443-005-1119-1.
[22] A.P. Mouritz, Advances in understanding the response of fibre-based polymer composites to shock waves and explosive blasts, Compos. Part A Appl. Sci. Manuf. 125 (2019) 105502, https://doi.org/10.1016/j.compositesa.2019.105502.
[23] H. Bornstein, S. Ryan, A. Mouritz, Physical mechanisms for near-field blast mitigation with fluid containers, in: A.P. Mouritz, Y.D.S. Rajapakse (Eds.), Explos. Blast Response Compos., Elsevier, Duxford, United Kingdom, 2017, pp. 345–374.